Materials Advances

ROYAL SOCIETY OF CHEMISTRY

PAPER

View Article Online
View Journal

Check for updates

Cite this: DOI: 10.1039/d5ma00397k

Mapping the L-tryptophan capped copper nanocluster mediated binding and targeted pH-responsive release of doxorubicin *via* fluorescence resonance energy transfer (FRET)†

Aarya,[a] Anna Sebastian,[a] Kavya P.,[a] Indrajit Bhattacharjee,[b] Abhishek S. Shekhawat,[c] Bibhu Ranjan Sarangi[bd] and Supratik Sen Mojumdar *[a]

Targeted delivery and controlled release of anticancer drugs pose significant challenges in effective cancer therapy. In this study, we developed a tryptophan-capped copper nanocluster (Trp-Cu NC) as a nano-drug carrier for the selective and pH-responsive release of the anticancer drug doxorubicin (Dox). The Trp-Cu NC exhibits substantial spectral overlap with Dox, forming an efficient fluorescence resonance energy transfer (FRET) pair that enables precise monitoring of drug binding interactions through both steady-state and time-resolved fluorescence measurements. Upon increasing the Dox concentration (~160 μM), the photoluminescence (PL) intensity and the lifetime of the Trp-Cu NC (donor) decreased significantly, indicating enhanced FRET efficiency (E_{FRET}) and reduced donor–acceptor distance (r_{DA}). The interaction between Trp-Cu NC and Dox under neutral pH resulted in the formation of a Trp-Cu NC–Dox nanoconjugate of diameter ~24.7 ± 1.1 nm meeting the size criterion suitable for good drug delivery performance. Under acidic conditions (pH 5.5), mimicking the tumor microenvironment, the Trp-Cu NC–Dox nanoconjugate dissociated back to the nanocluster (diameter ~2.7 ± 0.1 nm) releasing the drug, which translated into a remarkable increase in the Trp-Cu NC (donor) lifetime followed by a decreased E_{FRET}. Such a phenomenon was absent under physiological pH 7.4, making the Trp-Cu NC a suitable nano-carrier for targeted drug release in cancer cells. The cytotoxicity studies further corroborate that Trp-Cu NC can selectively release Dox to the cancer cells enhancing the therapeutic efficacy of the drug by ~3.6-fold, concurrently decreasing its toxicity appreciably towards normal cells. Overall, these findings substantiate an easy and economical strategy to develop a novel nano-drug carrier that offers selectivity and improved drug-release performance, potentially overcoming the systemic toxicity associated with conventional chemotherapy.

Received 24th April 2025,
Accepted 29th May 2025

DOI: 10.1039/d5ma00397k

rsc.li/materials-advances

1. Introduction

Cancer has emerged as one of the leading causes of death worldwide over the past few decades.[1] Although conventional treatments such as chemotherapy and radiation therapy have advanced over the years and are effective in many cases, they still face significant challenges.[2] One of the major limitations is the lack of selectivity and specificity of cytotoxic anticancer drugs, which often damage healthy tissues along with cancerous ones.[3] Due to their non-specific distribution, only a tiny fraction of these drugs reach the tumor site, where absorption by the tumor cells is often poor. This necessitates higher dosages, increasing the risk of severe side effects.[4] Enhancing the selectivity and specificity of anticancer agents toward tumor tissues could reduce the required drug dosage and minimize adverse effects.[5,6] Doxorubicin (Dox), a widely used chemotherapeutic agent, is employed in the treatment of various cancers, including breast,[4] lung,[7] bone,[8] and stomach cancers.[9] However, its direct administration is associated with several drawbacks, such as acute cardiotoxicity, limited tumor-targeting capability, poor bioavailability, and the development of drug resistance.[4,10] Therefore, novel strategies are urgently needed to deliver Dox more

[a] Department of Chemistry, Indian Institute of Technology Palakkad, Kerala, 678 623, India. E-mail: supratik@iitpkd.ac.in
[b] Department of Physics, Indian Institute of Technology Palakkad, Kerala, 678 623, India
[c] Department of Physics, SRM Institute of Science and Technology, Tamil Nadu, 603 203, India
[d] Department of Biological Sciences and Engineering, Indian Institute of Technology Palakkad, Kerala, 678 623, India

† Electronic supplementary information (ESI) available. See DOI: https://doi.org/10.1039/d5ma00397k

effectively—minimizing its toxicity while retaining its therapeutic efficacy in cancer treatment.

In recent decades, nanoscale materials have garnered significant interest due to their exceptional physicochemical and optoelectronic characteristics, which render them suitable for a vast array of interdisciplinary applications.[11,12] Metal nanoclusters (NCs) are among such emerging classes of fluorescent nanomaterials with intriguing properties, including strong photoluminescence, tuneable fluorescence emission, good quantum yield, high photochemical stability, long emission lifetime, low cytotoxicity and easy synthesis.[13,14] As the size of the metal nanoclusters approaches close to the Fermi wavelength of an electron (typically <2 nm), discrete energy levels emerge, leading to size-tunable electronic transitions.[5] Furthermore, the properties of nanoclusters can be precisely tuned through surface functionalization using a variety of ligands, including proteins,[15,16] small molecules,[17,18] amino acids,[19,20] DNA,[21,22] polymers[23,24] *etc.* These modifications allow for the development of highly versatile nanoprobes with significant potential in novel therapeutic applications.[6,25,26]

Owing to their low cytotoxicity, biodistribution and easy clearance, bio-molecule functionalized noble metal NCs could act as a potential nano-drug carrier for the selective delivery and controlled release of anticancer drugs.[13] These NCs offer a versatile and adaptable platform for cancer cell imaging, making them highly suitable for targeted therapy.[14,27] Their ultra-small size provides a high surface-to-volume ratio, enhancing drug binding and therapeutic efficacy.[28] Unlike many conventional drug carriers, metal nanoclusters possess the additional advantage of efficient renal clearance due to their ultrasmall dimensions.[27] Moreover, the inherent luminescence of metal nanoclusters facilitates real-time monitoring of drug binding and release.[29,30] For *in vivo* applications, NCs capped with smaller biomolecules, such as amino acids, are particularly advantageous due to their excellent biocompatibility, straightforward structure, high stability, amphoteric nature, and ability to integrate seamlessly into biological systems.[19,31,32] Among various natural amino acids, tryptophan stands out as it is abundantly present in transmembrane proteins, where it plays a crucial role in anchoring to membranes and promoting endocytosis—a key mechanism for cellular uptake.[33] Tryptophan exhibits a higher affinity for crossing the blood–brain barrier compared to other amino acids, making it an attractive candidate for the development of nanocluster-based drug delivery systems.[34]

Copper, a vital component of several metalloproteins and an earth-abundant, cost-effective metal, has been widely studied for nanocluster synthesis.[35] Although its high oxidation potential poses challenges compared to noble metals like gold and silver, appropriate templates can yield stable copper nanoclusters (Cu NCs) with diverse functionalities.[30] Tryptophan has emerged as an excellent scaffold for Cu NCs, offering good biocompatibility, strong photoluminescence, and high photostability.[19,36] Its small molecular size also facilitates cellular uptake, making tryptophan-capped Cu NCs (Trp-Cu NCs) effective nanoprobes for cell imaging.[19,36] Given these attributes, Trp-Cu NC could thus be a highly proficient nano-probe for *in-vivo* drug delivery and release compared to the other protein/polymer functionalized nanoclusters.[6,25,27,37,38] Additionally, the emission spectrum of Trp-Cu NC significantly overlaps with the absorption spectrum of an anticancer drug Dox, making it an excellent FRET pair enabling easy monitoring of the drug binding and release.[19]

Fluorescence resonance energy transfer (FRET) has been widely used as a ''spectroscopic ruler'' to measure distances (<10 nm) between two fluorophores with high sensitivity.[39,40] It relies on long-range (<10 nm) dipole–dipole interactions and is highly dependent on the spatial proximity between the donor and acceptor.[41,42] FRET efficiency and donor–acceptor distance can be estimated from changes in fluorescence intensity or excited-state lifetime.[41,43] A critical requirement for FRET is significant spectral overlap between the fluorophores, making the selection and design of suitable FRET pairs essential.[44] Since this specific criterion cannot be achieved between any randomly chosen fluorophores, the real challenge lies in the design of a suitable FRET pair assembly.[28] FRET is particularly valuable in drug delivery research for tracking nanoparticle–drug interactions.[45] The energy transfer efficiency directly reflects the distance between the nanocarrier and the drug, providing insight into drug binding and release.[25,28] This enables comprehensive evaluation of a nanoparticle's effectiveness as a drug carrier and sheds light on drug fate during nano–bio interactions.[28]

In this study, Trp-Cu NC was employed as a nano-drug carrier for the targeted release of the anticancer drug, Dox, specifically to cancer cells. The binding interaction between Trp-Cu NC and Dox was monitored using both steady-state and time-resolved FRET. At neutral pH (7.0), Trp-Cu NC exhibited strong binding with Dox, forming larger nanoconjugates. This interaction was confirmed by relatively higher FRET efficiency and drug-binding metrics. Drug release was evaluated through a pH-dependent study. At acidic pH (5.5), mimicking the tumor microenvironment,[46,47] a notable decrease in FRET efficiency indicated effective drug release, while no change in FRET efficiency was observed at physiological pH (7.4). The *in vitro* drug release profile further highlights the nanocluster's enhanced ability to release Dox in acidic cancerous environments selectively. Cell viability assays further supported the system's effectiveness, demonstrating targeted cancer cell killing at lower drug concentrations, while sparing normal cells even at higher concentrations. This suggests that Trp-Cu NC enhances the therapeutic efficacy of Dox while minimizing side effects. Overall, this work demonstrates that Trp-Cu NC is a simple, cost-effective, and efficient nano-drug carrier for targeted cancer therapy. Moreover, FRET-based real-time monitoring of drug loading and release *in vitro* offers valuable insights into pharmacokinetics and pharmacodynamics, paving the way for future theranostic applications.

2. Experimental section

2.1. Materials

L-Tryptophan (Scheme 1(A)) used as a scaffold for the synthesis of Trp-Cu NC was purchased from Sisco Research Laboratories Pvt., Ltd (SRL). Copper chloride ($CuCl_2$), sodium hydroxide

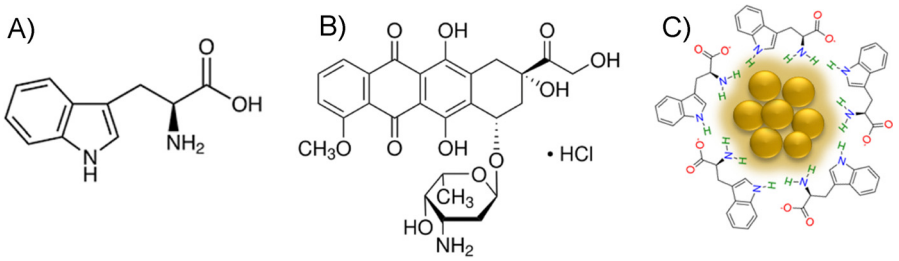

Scheme 1 Structure of (A) L-tryptophan (Trp) and (B) doxorubicin hydrochloride (Dox), and schematic representation of (C) Trp-Cu NC.

(NaOH) and hydrazine monohydrate ($N_2H_4{\cdot}H_2O$) were purchased from Nice Chemicals. Doxorubicin hydrochloride (Dox) (Scheme 1(B)) used for the FRET study was purchased from Tokyo Chemical Industry (TCI). The following chemicals used for the preparation of buffer solutions were purchased either from Nice Chemicals or SRL: sodium dihydrogen orthophosphate ($NaH_2PO_4{\cdot}2H_2O$), disodium hydrogen orthophosphate anhydrous (Na_2HPO_4), sodium acetate (CH_3COONa), hydrochloric acid (HCl) and acetic acid (CH_3COOH). All the solutions were prepared using doubly distilled water from the Biopak Polisher Milli-Q water system (CDUFB1001). MTT dye was purchased from SRL, and dimethyl sulfoxide (DMSO) was purchased from HiMedia. 3T3 and MCF-7 cell lines were obtained from the Cell Repository, National Centre for Cell Science (NCCS), Pune, India. All the reagents purchased were used without any further purification.

2.2. Formation of the Trp-Cu NC–Dox nanoconjugate

The Trp-Cu NC was synthesized following a previously reported protocol.[19] The diluted (~5 times) solution of Trp-Cu NC (2 mL) (Scheme 1(C)) after adjusting the pH to 7 was heated at 37 °C for 15-minute and the emission spectra were recorded. Then 20 μM of Dox (31 μL from 1.3 mM stock solution) each were added successively in a 15-minute time interval to the same solution of NC with continuous stirring under the same temperature. The steady-state PL emission spectra (λ_{ex} = 380 nm), as well as time-resolved photoluminescence decay curves (λ_{ex} = 405 nm, λ_{em} = 480 nm) of the NC, were recorded successively. After attaining a final concentration of 160 μM of Dox in the NC solution, the reaction mixture was allowed to age overnight at 37 °C. The so-synthesized Trp-Cu NC–Dox nanoconjugate was further collected by centrifugation at 14 000 × *g* for 30 minutes, washed, and redispersed in 2 mL Milli-Q water for further use.

2.3. Instrumentation

Steady-state fluorescence emission spectra were recorded using the PerkinElmer fluorescence spectrometer (FL 8500). The L-tryptophan capped copper nanocluster was excited at 380 nm and the spectra were scanned from 390 to 700 nm at a scan rate of 240 nm min^{-1} with excitation and emission slit widths at 5 nm and an emission filter at 430 nm. UV-visible absorption spectra of Dox were recorded using a Thermo Fischer Scientific (Evolution 201) UV-vis spectrophotometer. The morphology of the Trp-Cu NC–Dox nanoconjugate was studied on a field emission scanning electron microscope (FESEM) from Carl Zeiss, Germany (model no. Gemini SEM 300). The samples were drop-cast over a silicon wafer and dried overnight before the analysis. The size of the Trp-Cu NC–Dox nanoconjugate under acidic pH was determined using a high-resolution transmission electron microscope (HRTEM) from JEOL, Japan (model no. JEM-2100 Plus) after drop-casting the samples on a carbon-coated copper grid followed by drying overnight. An IR Tracer-100 FTIR spectrophotometer from Shimadzu Scientific Instruments was used to record the Fourier transform infrared (FTIR) spectra. The samples were scanned from 4000–399 cm^{-1} at 0.2 cm^{-1} resolution. Time-resolved photoluminescence intensity decay of the NC was recorded on a time-correlated single-photon counting (TCSPC) setup (HORIBA, Deltaflex) using a 405 nm pulsed laser diode with a typical pulse width of 90 ps. Dynamic light scattering (DLS) and zeta potential measurements were done using a Zetasizer Nano-ZS (Malvern Panalytical, UK). The Trp-Cu NC–Dox nanoconjugates were collected by centrifugation using a non-refrigerated centrifuge from Dinesh Scientific (Model No: DS-NRC-473).

2.4. *In vitro* release of Dox from the Trp-Cu NC–Dox nanoconjugate

Initially the phosphate buffer solution at pH 7.4 and acetate buffer solution at pH 5.5 were prepared. Then the Trp-Cu NC–Dox nanoconjugates were dispersed separately in 2 mL each of the buffer solutions and both solutions were incubated at room temperature for 24 hours. The time-resolved photoluminescence decay curve (λ_{ex} = 405 nm, λ_{em} = 480 nm) was recorded immediately after the addition as well as after 24 hours of incubation. The *in vitro* drug release profile of Dox from the Trp-Cu NC–Dox nanoconjugate was evaluated by incubating the purified nanoconjugate separately in 2 mL of phosphate buffer (pH 7.4) and acetate buffer (pH 5.5). The samples were placed in a dialyzer tube (Tube-O-DIALYZER, 1 kDa MWCO, G-Biosciences) and immersed in 100 mL of the respective buffer under continuous stirring at 37 °C. At predetermined time intervals, the concentration of Dox in the dialysis tube was determined by measuring its absorbance at 480 nm, and the cumulative drug release percentage was subsequently calculated.[5,25]

2.5. Calculation of fluorescence resonance energy transfer (FRET) parameters

The magnitude of spectral overlap was determined from the spectral overlap integral, $J(\lambda)$ using the expression,[44]

$$J(\lambda) = \frac{\int_0^\infty F(\lambda)\cdot\varepsilon(\lambda)\cdot\lambda^4 d\lambda}{\int_0^\infty F(\lambda) d\lambda} \quad (1)$$

where $F(\lambda)$ is the fluorescence intensity of the donor Trp-Cu NC at wavelength λ and ε is the molar extinction coefficient of the acceptor at wavelength λ. From the $J(\lambda)$ thus obtained, the Förster distance R_0, the critical donor–acceptor distance at which the FRET efficiency is 50%, can be calculated using the equation,[44]

$$R_0 = 0.0211[J(\lambda)\cdot\kappa^2\cdot\eta^{-4}\cdot\phi] \text{ (in nm)} \quad (2)$$

where κ^2 is the orientation factor commonly considered as 2/3 for random orientation, η is the refractive index of the medium, and ϕ is the quantum yield of the donor Trp-Cu NC. The quantum yield (ϕ) of the Trp-Cu NC was measured following the method described earlier using quinine hemi-sulphate ($\phi \sim 0.546$) as the reference.[15] The steady-state based FRET efficiency (E_{FRET}) can be calculated from the PL intensity of Trp-Cu NC in the presence (F_{DA}) and absence (F_D) of Dox using the formula:[44]

$$E_{FRET} = 1 - \frac{F_{DA}}{F_D} \quad (3)$$

The E_{FRET} can also be calculated from the average lifetime of Trp-Cu NC in the presence (τ_{DA}) and absence (τ_D) of Dox using the formula,[44]

$$E_{FRET} = 1 - \frac{\tau_{DA}}{\tau_D} \quad (4)$$

The E_{FRET} also depends upon the parameters R_0 and r, where r is the actual distance between the donor and acceptor and is given by the equation,[44]

$$E_{FRET} = \frac{R_0^6}{R_0^6 + r_{DA}^6} \quad (5)$$

Knowing the E_{FRET} and R_0, the donor–acceptor distance (r_{DA}) can be calculated using the formula,

$$r_{DA} = R_0 \times \left(\frac{1 - E_{FRET}}{E_{FRET}}\right)^{\frac{1}{6}} \quad (6)$$

The rate of energy transfer $k_T(r)$ from donor to acceptor can be determined using the equation,[44]

$$k_T(r) = \frac{1}{\tau_D}\left(\frac{R_0}{r_{DA}}\right)^6 \quad (7)$$

2.6. Cell viability and imaging studies

To monitor the viability of the normal (3T3 mouse fibroblast) and cancer (MCF-7 breast cancer) cells against the free Dox and Trp-Cu NC–Dox nanoconjugate, an MTT-based assay was done following the protocol mentioned earlier.[15,19] Briefly, the 3T3 and MCF-7 cells were incubated with varying concentrations (0.25–40 μM) of free Dox and Dox bound to the Trp-Cu NC in the nanoconjugate for 24 h. After incubation, MTT was added to each well (final concentration $\sim$0.5 mg mL^{-1}). The resulting formazan crystals were dissolved in dimethyl sulfoxide (DMSO) and the absorbance was recorded in a plate reader (Biotech Epoch 2NS Gen5) at 590 nm using a 620 nm reference filter. The viability thus obtained was normalized for each concentration. The IC_{50} values were determined by fitting the dose–response cell viability data to a sigmoidal curve. For imaging, the cells were incubated with $\sim$5 μM Trp-Cu NC–Dox for 6 hours. Post-incubation cells were fixed using *para*-formaldehyde. Imaging was done using a confocal microscope (Olympus Fluoview fv3000) with suitable excitation and emission parameters.

2.7. Error analysis

All the reported errors in this study represent the standard error of the mean (s.e.m. = $\sigma/\sqrt{n}$, where σ is the standard deviation and n is the number of measurements) calculated from at least three or more independent measurements ($n \geq 3$). Statistical significance (p-values) was assessed using a two-sample t-test.

3. Results and discussion

3.1. Interaction of Trp-Cu NC with doxorubicin studied *via* FRET

The synthesized L-tryptophan scaffolded copper nanoclusters (Trp-Cu NCs), with spherical morphology and an average diameter of 2.5 ± 0.2 nm (Fig. 1(A)), exhibited strong photoluminescence (λ_{ex}^{max} = 380 nm, λ_{em}^{max} = 500 nm) (Fig. 1(B)) and a quantum yield (ϕ) of approximately 0.114.[19] These NCs have demonstrated excellent stability, resistance to oxidative damage, biocompatibility, and suitability for live cell imaging.[19] Their ultrasmall size, combined with the membrane-anchoring capability of the tryptophan scaffold, facilitates efficient cellular uptake.[19] Trp-Cu NCs thus hold promise as nano-drug carriers, provided they can bind and release drug molecules at targeted sites. Notably, their emission spectrum exhibits excellent spectral overlap with the absorption spectrum of the anticancer drug doxorubicin (Dox), establishing them as an ideal FRET pair.[19] This enables effective monitoring of nanocluster–drug interactions *in vitro via* fluorescence resonance energy transfer (FRET). The estimated Förster distance (R_0) of 3.2 nm, derived from the spectral overlap, falls well within the optimal range (<10 nm) for an ideal FRET pair.[19]

To investigate the interaction between Trp-Cu NC and Dox, increasing concentrations of Dox (up to $\sim$160 μM, in $\sim$20 μM increments) were gradually added to diluted aqueous solution of Trp-Cu NC at neutral pH ($\sim$7). The mixture was stirred at 37 °C for 15 minutes, and the PL emission spectra (λ_{ex} = 380 nm) were recorded (Fig. 2(A)). Upon Dox addition, the emission maxima of Trp-Cu NC exhibited a significant blue shift, indicating a more hydrophobic environment around the nanocluster induced by Dox.[48] Moreover, a notable decrease in the PL intensity of the Trp-Cu NC (donor) was accompanied by a corresponding increase in the emission intensity of Dox (acceptor) at 590 nm (Fig. 2(A)), consistent with efficient FRET. The FRET efficiency (E_{FRET}), calculated based on PL intensity changes, increased with Dox concentration and plateaued at $\sim$160 μM, reaching a maximum efficiency of $\sim$84.5 ± 3%. This corresponds to an average donor–acceptor distance (r_{DA}) of

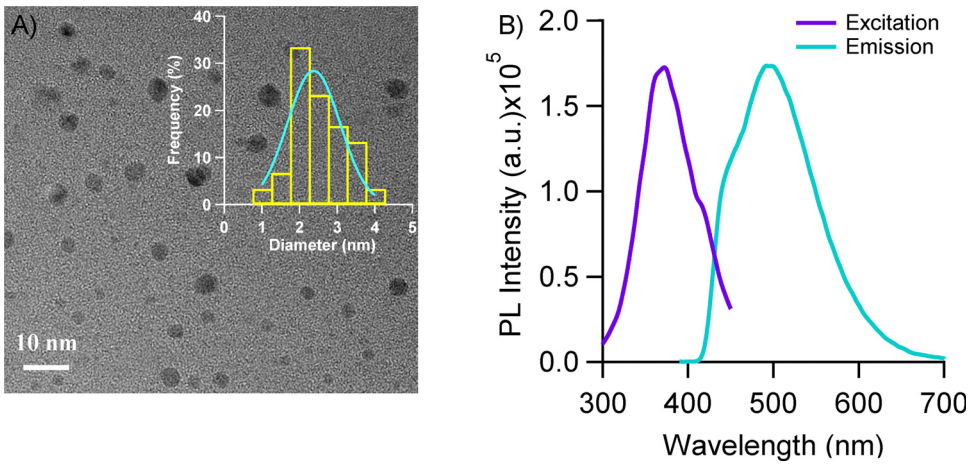

Fig. 1 (A) High-resolution transmission electron microscopy (HRTEM) image of Trp-Cu NCs. The inset shows the corresponding size distribution (number of particles analysed (N) = 110) obtained from the HRTEM image. (B) Excitation (λ_{em} = 500 nm) (violet) and emission (λ_{ex} = 380 nm) (cyan) spectra of Trp-Cu NC.

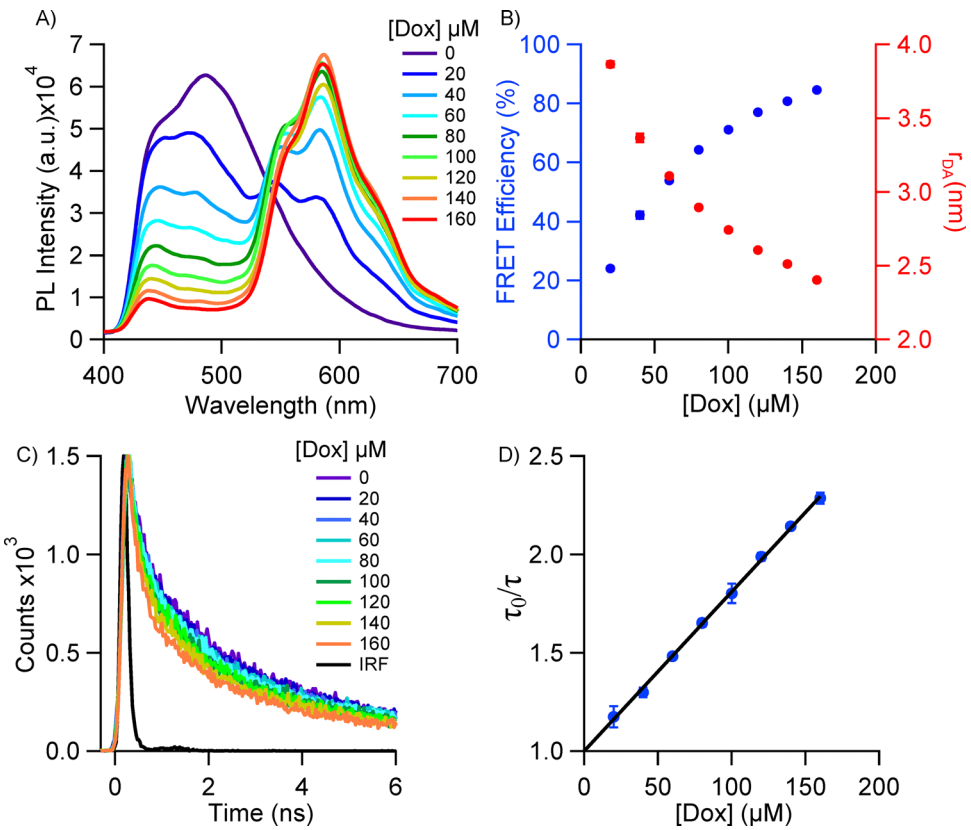

Fig. 2 (A) Emission spectra (λ_{ex} = 380 nm) of Trp-Cu NC in the presence of increasing concentrations of doxorubicin (Dox). (B) Changes in the steady-state-based FRET efficiency (blue) and donor–acceptor distance (r_{DA}) (red) at varying concentrations of Dox. (C) Time-resolved PL intensity decay curve of Trp-Cu NC (λ_{ex} = 405 nm, λ_{em} = 480 nm) in the presence of increasing concentrations of Dox. The black curve represents the instrument response function (IRF). (D) Lifetime-based Stern–Volmer plot (blue) with a linear fit (black).

2.4 ± 0.01 nm (Fig. 2(B)), indicating an increased number of Dox molecules bound to the surface of the Trp–Cu nanocluster.

To gain deeper insights into the FRET between Trp-Cu NC and Dox, steady-state PL measurements were complemented with time-resolved fluorescence studies. A similar trend was observed: as the Dox concentration increased, the average lifetime of Trp-Cu NC decreased from 2.0 ± 0.05 ns (in the absence of Dox) to 0.9 ± 0.02 ns at 160 μM Dox. This corresponded to a maximum E_{FRET} of ~56.2 ± 1% and an average nanocluster-Dox distance (r_{DA}) of 3.0 ± 0.02 nm

(Fig. 2(C) and Fig. S1, ESI†). Initially, differences in E_{FRET} and r_{DA} values were observed between the steady-state and time-resolved measurements. Steady-state FRET often overestimates the efficiency due to the potential direct excitation of the acceptor and the resulting inner filter effect. In contrast, time-resolved FRET is more reliable, as it depends solely on the donor's lifetime rather than fluorescence intensity. However, after aging the sample overnight, these differences diminished, and both methods yielded comparable FRET efficiencies—$\sim$80 $\pm$ 4.6% (steady-state) and $\sim$74 $\pm$ 4.4% (time-resolved)—with respective average donor–acceptor distances of 2.5 $\pm$ 0.1 nm and 2.7 $\pm$ 0.1 nm (Fig. S2, ESI†). These distances fall within the optimal FRET range ($0.5R_0 < r < 2R_0$).[42,49]

This initial discrepancy in the E_{FRET} and r_{DA} values obtained from the steady-state and time-resolved measurements can be ascribed to the diffusion of the unreacted nanocluster and the dye molecules, in addition to the direct excitation of the acceptor. Diffusion plays an important role in the FRET process.[50,51] Using the Stokes–Einstein equation,[52] $D = \frac{k_B T}{6\pi\eta r}$ (where k_B is the Boltzmann's constant, T is the temperature, η is the viscosity of the medium and r is the hydrodynamic radius of the diffusing particle) the diffusion coefficient of both the Trp-Cu NC (diameter $\sim$ 2 nm) and Dox (diameter $\sim$ 1.5 nm) can be readily estimated to be 218 $\mu m^2\ s^{-1}$ and 284 $\mu m^2\ s^{-1}$, respectively. Successively the average distance travelled by the molecules during the FRET process can also be calculated from their average lifetime τ ($\sim$1 ns) and diffusion coefficient D using the equation,[53] $x = \sqrt{D\tau}$, and it was determined to be 0.4 nm and 0.5 nm for Trp-Cu NC and Dox, respectively. In time-resolved measurements, the molecules are typically exposed to an ultrashort laser pulse of $<$1 ns width. Since their diffusion is much slower compared to their lifetime, they almost remain stationary during that period; as a result, the effect of diffusion on the energy transfer calculated from the lifetime was negligible.[42,50,51] On the contrary, during the steady-state measurements, the sample is exposed to a continuous light source; hence, more donor and acceptor molecules have enough time to diffuse into the sphere of diameter $<$10 nm, a preferable distance for FRET, resulting in a higher energy transfer.[42,51] After aging, this effect due to diffusion was less prominent since the number of free nanocluster and dye molecules significantly decreased upon forming the Trp-Cu NC–Dox nanoconjugate.

The binding efficiency (BE) reflects the fraction of the drug bound to the nanocluster, and is calculated using the equation,[5]

$$BE\% = \frac{W_{\text{drug in nanocarrier}}}{W_{\text{total drug}}} \times 100$$

where W refers to the weight of Dox in $\mu g\ mL^{-1}$. The concentration of unbound Dox in the supernatant of the Trp-Cu NC–Dox nanoconjugate (after overnight aging) was determined by measuring the absorbance at 480 nm, yielding a binding efficiency of 69%—comparable to other established drug carriers.[5,54,55] Following purification to remove unreacted nanoclusters and free Dox, the time-resolved FRET efficiency (E_{FRET}) increased markedly to $\sim$98 $\pm$ 1%, with a reduced donor–acceptor distance (r_{DA}) of $\sim$1.65 $\pm$ 0.1 nm (Fig. S2, ESI†), suggesting close proximity of Dox to the nanocluster surface. The corresponding energy transfer rate constant ($k_{FRET}(r)$) was calculated to be $\sim 2.7 \times 10^{10}\ s^{-1}$. A lifetime-based Stern–Volmer plot (τ_0/τ *vs.* [Dox], where τ_0 is the average lifetime of the donor alone and τ is in the presence of acceptor) fits well to the linear equation, $\frac{\tau_0}{\tau} = 1 + K_{SV}[Q]$ (where [Q] is the quencher concentration and K_{SV} is the Stern–Volmer constant), yielding a Stern–Volmer constant (K_{SV}) of $8 \times 10^3\ M^{-1}$ (Fig. 2(D)). The corresponding bimolecular quenching constant (k_q) $\left(k_q = \frac{K_{SV}}{\tau_0}\right)$ was calculated as $4 \times 10^{12}\ M^{-1}\ s^{-1}$, indicating that quenching occurs *via* pre-binding interactions between Trp-Cu NC and Dox.[42,56] These time-resolved fluorescence results strongly corroborate the steady-state FRET data, further confirming the active and specific interaction between the nanocluster and the drug.

The small r_{DA} value between Trp-Cu NC and Dox indicates close proximity, suggesting strong surface interaction and possible complex formation. Consequently, visible aggregates were observed in the aged sample. Field emission scanning electron microscopy (FESEM) analysis was carried out to examine these structures. FESEM images revealed rod-like aggregates (Fig. 3(A) and Fig. S3A, ESI†), which on closer inspection were found to result from the alignment of larger nanoconjugates into elongated structures (Fig. 3(B)). The average diameter of these individual nanoconjugates was $\sim$24.7 $\pm$ 1.1 nm (Fig. 3(C)), approximately 10 times larger than the original spherical nanoclusters ($\sim$2.5 $\pm$ 0.2 nm) ($p < 0.0005$) (Fig. 1(A)). The binding of Dox to the Trp-Cu NC surface induced a morphological shift from spherical to non-spherical structures as evident in Fig. 3(B). Each nanoconjugate likely consists of multiple Trp-Cu NCs and Dox molecules in an aggregated form organized in an elongated manner. The FESEM results were further supported by high-resolution transmission electron microscopy (HRTEM) (Fig. 3(D) and Fig. S3B, ESI†). The HRTEM images also revealed elongated rod-shaped structures, typically measuring approximately between 80–160 nm in length and 30–40 nm in width. Each rod-shaped structure appears to be composed of smaller rod-like units with widths of around 4 nm. The slight variations in the appearance of the FESEM and HRTEM images can be attributed to differences in imaging techniques and resolution. Although dynamic light scattering (DLS) analysis is not ideal for characterizing rod-shaped particles, the results suggest the presence of particles with a hydrodynamic diameter approximately in the 160 nm range (Fig. S4, ESI†). Particles within the 10–200 nm size range are ideal for drug delivery to tumour tissues *via* the enhanced permeability and retention (EPR) effect.[27,54] Accordingly, the Dox-loaded nanoconjugates meet this criterion, making them well-suited for efficient passive targeting and drug release. These findings collectively confirm strong and stable interactions between Trp-Cu NC and Dox.

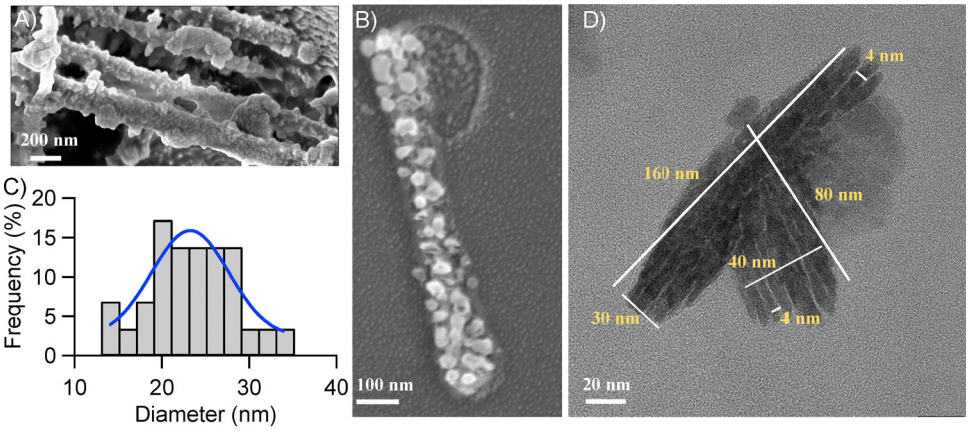

Fig. 3 (A) FESEM image of purified Trp-Cu NC–Dox nanoconjugates. (B) Magnified FESEM image of the rod-shaped aggregate formed by a congregation of individual Trp-Cu NC–Dox nanoconjugates. (C) Particle size distribution (N = 57) of individual nanoconjugates forming rod-shaped structures. (D) HRTEM image of the purified Trp-Cu NC–Dox nanoconjugates.

The binding of Dox onto the nanocluster surface was further confirmed by the Fourier transform infrared (FTIR) spectra (Fig. 4(A)). The variations in the position and intensity of the vibration bands can be attributed to the participation of various functional groups in the formation of intermolecular bonds.[57] The broad band observed in the range of 3000–3600 cm^{-1} was due to the N–H and O–H stretching vibrations commonly present in both NC and Dox.[15,55,57] The sharp peak at 1640 cm^{-1} present in both Dox and NC can be ascribed to the C=O stretching vibrations.[15,55,57] The FTIR spectra of the Trp-Cu NC–Dox nanoconjugate before aging showed a close resemblance with that of pure Trp-Cu NC but after aging and purification subtle differences in the spectra can be identified. The characteristic bands present in pure Trp-Cu NC and Dox can still be partially observed in the aged and purified Trp-Cu NC–Dox nanoconjugate indicating the conjugation of Dox onto the nanocluster. However, a stark difference could be observed around the 3000–3600 cm^{-1} region, a much weaker band in this region after the formation of the Trp-Cu NC–Dox nanoconjugate suggests the involvement of nitrogen and oxygen atoms, playing a pivotal role in the complex formation. At neutral pH, Trp (pI ~ 5.9) remains mostly negatively charged while Dox (pK_a ~ 8.2) remains positively charged, and thus a strong electrostatic interaction is expected between them mainly involving the nitrogen and oxygen atoms.[58] The near-zero zeta potential value (−0.08 mV) of the Trp-Cu NC–Dox nanoconjugate supports the involvement of electrostatic interactions, resulting in overall charge neutrality. This further promotes the self-aggregation of the conjugates into rod-shaped structures. The appearance of a new band around 1520 cm^{-1} along with the characteristic C=O stretching peak at 1630 cm^{-1} can be attributed to the N–H bending vibration.[15] Furthermore, the new peaks that emerged around 1000–1400 cm^{-1} for the aged and purified Trp-Cu NC–Dox nanoconjugate can be assigned to the formation of new bonds between the Trp-Cu NC and Dox, presumably C–O (1000–1300 cm^{-1}) and C–N (1000–1250 cm^{-1}) bonds (Fig. 4(A)).[15,55,57]

The binding constant of the interaction of Dox with Trp-Cu NC was evaluated from the Benesi–Hildebrand equation:[59,60]

$$\frac{1}{F_0 - F} = \frac{1}{(F_0 - F')}\frac{1}{K[Q]} + \frac{1}{F_0 - F'}$$

where F and F_0 are the PL intensity of Trp-Cu NC in the presence and absence of Dox respectively, F' is the PL intensity

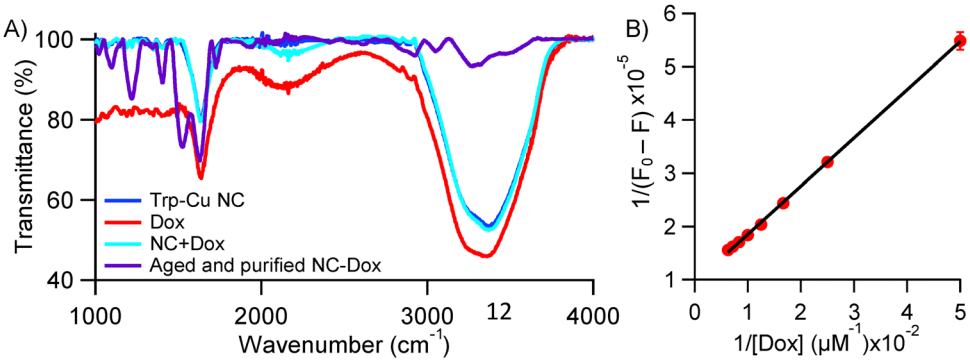

Fig. 4 (A) FTIR spectra of Trp-Cu NC (blue), free Dox (red), Trp-Cu NC + 160 μM Dox before aging (cyan) and aged and purified Trp-Cu NC–Dox nanoconjugate (violet). (B) Benesi–Hildebrand plot to determine the binding constant.

of Trp-Cu NC at the maximum concentration of Dox, [Q] is the concentration of Dox and K is the binding constant, which can be obtained by dividing the intercept $(1/(F_0 - F'))$ by the slope of the curve $(1/K\,(F_0 - F'))$.[59] The intercept and slope of the curve were measured to be 9.5×10^{-6} and 9×10^{-10} M, respectively (Fig. 4(B)). The binding constant determined using the given equation was 1.06×10^4 M^{-1}. A significantly higher value of binding constant indicates the stronger interaction existing between NC and Dox which is consistent with the FESEM images.

3.2. pH-responsive release of Dox from the Trp-Cu NC–Dox nanoconjugate

The pH-responsive *in vitro* release of Dox from the Trp-Cu NC–Dox nanoconjugates was qualitatively assessed using a FRET study. Aged and purified nanoconjugate samples were incubated in buffer solutions of pH 5.5 (acidic, mimicking the tumour microenvironment),[46,47] and the physiological pH of 7.4 (physiological pH of normal cells). The photoluminescence lifetime of Trp-Cu NC was measured immediately after buffer addition and again after overnight incubation. A marked increase in an average lifetime—from 0.03 ± 0.01 ns to 0.8 ± 0.1 ns—was observed at pH 5.5 indicating reduced E_{FRET} due to increased donor–acceptor distance upon drug release. In contrast, the lifetime remained nearly unchanged at pH 7.4 (Fig. 5(A)), suggesting minimal release under normal physiological conditions. This 'FRET-OFF' response qualitatively demonstrates the utility of FRET as a tool for monitoring drug release. Quantitative analysis of the *in vitro* release profile further revealed ~84% cumulative Dox release at pH 5.5 after 28 hours, compared to ~53% at pH 7.4 ($p < 0.005$) (Fig. 5(B)), validating the nanoconjugate's pH-sensitive release profile.

pH-induced bond cleavage is a widely adopted strategy for targeted drug release.[58] At acidic pH (5.5), protonation of nitrogen and oxygen atoms in the Trp scaffold reduces the net negative charge on the nanocluster surface, thereby weakening electrostatic interactions with Dox and facilitating bond cleavage for drug release.[58] Additionally, lower pH may disrupt hydrogen bonding between Dox and Trp-Cu NC, further promoting release.[58] In contrast, *in vitro* drug release assays show significantly less release under physiological conditions, highlighting the nanoconjugate's selective release behaviour. This pH-dependent release may improve therapeutic efficacy while reducing off-target toxicity—a major drawback of conventional chemotherapy.

The high-resolution transmission electron microscopy (HRTEM) images further corroborate the drug release at the acidic pH (pH 5.5). The HRTEM images of the Trp-Cu NC–Dox nanoconjugates incubated overnight at pH 5.5 showed a drastic reduction in the particle size when compared with the Trp-Cu NC–Dox nanoconjugates at neutral pH, the diameter of the particles decreased from 24.7 ± 1.1 nm to 2.7 ± 0.1 nm ($p < 0.0005$) (Fig. 6) matching nicely to the pure Trp-Cu NC (~2.5 ± 0.2 nm) (Fig. 1(A)) without the drug. This size reduction clearly suggests that upon incubating the nanoconjugates overnight under acidic conditions, the bound drug was released from the NC. Apart from this, the morphology of the particles also became spherical. Thus, there is almost complete regaining of the Trp-Cu NC without much destruction in the shape and size after the removal of Dox. All this experimental evidence indicates the potential selective and pH-responsive release of Dox into cancer cells by Trp-Cu NC. Hence, Trp-Cu NC is an excellent potent nano-drug carrier that can be utilized in the future for intracellular drug-delivery applications.

3.3. Trp-Cu NC–Dox nanoconjugate: selective killing of cancer cells

To evaluate the potential of Trp-Cu NC as a nano-drug carrier for the selective release of Dox to cancer cells, we compared the cytotoxic effects of free Dox and Trp-Cu NC–Dox nanoconjugates on both normal mouse fibroblast (3T3) and breast cancer (MCF-7) cells. Previous studies have demonstrated the biocompatibility of Trp-Cu NC with 3T3 cells across a wide concentration range, highlighting its suitability for biomedical

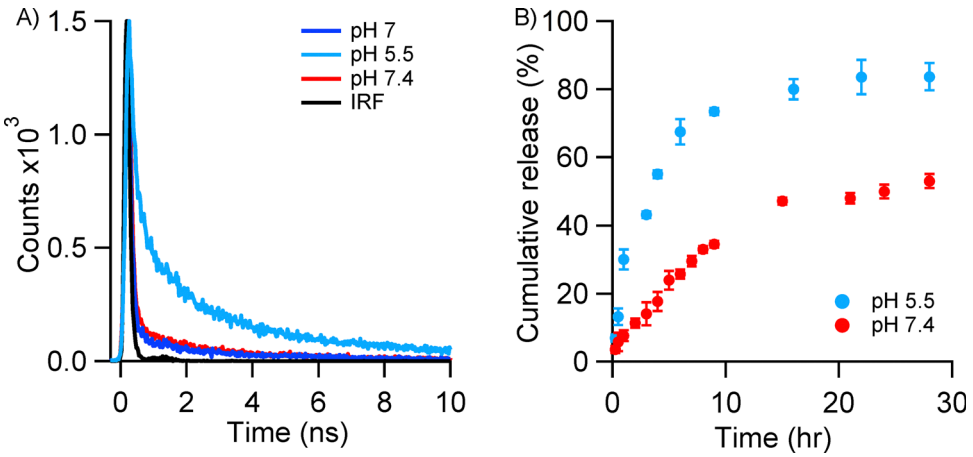

Fig. 5 (A) Time-resolved PL intensity decay curve of the aged and purified Trp-Cu NC–Dox nanoconjugate (λ_{ex} = 405 nm, λ_{em} = 480 nm) at pH 7 (blue), pH 5.5 (light blue) and pH 7.4 (red). The black curve represents the instrument response function (IRF). (B) Time-dependent *in vitro* release profile (%) of Dox from the Trp-Cu NC–Dox nanoconjugate at pH 5.5 (light blue) and pH 7.4 (red).

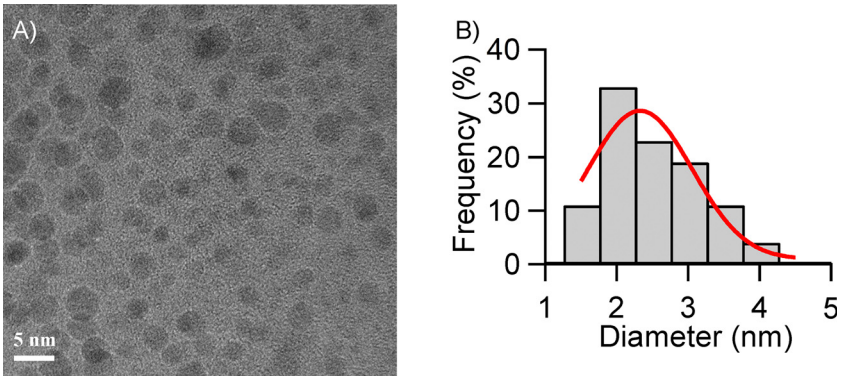

Fig. 6 (A) HRTEM image of aged and purified Trp-Cu NC–Dox nanoconjugates after overnight incubation at pH 5.5. (B) Particle size distribution (N = 101) obtained from the HRTEM image.

applications.[19] Furthermore, Trp-Cu NC readily internalizes into cells, making it highly suitable for applications in cell imaging and drug delivery.[19] Confocal microscopy of 3T3 cells incubated with Trp-Cu NC–Dox revealed cytosolic localization, confirming that the nanoconjugate can undergo internalization (Fig. S5, ESI†). Notably, the Trp-Cu NC–Dox nanoconjugate exhibited pronounced cytotoxicity towards MCF-7 cancer cells. At a concentration of ~10 μM, the conjugated Dox resulted in ~80% cancer cell death, while ~70% of 3T3 cells remained viable, indicating more selective toxicity toward cancer cells (Fig. 7). In contrast, the same concentration of free Dox killed only ~20% of the cancer cells, suggesting that conjugation with Trp-Cu NC significantly enhances Dox's therapeutic efficacy (Fig. 7(A)). This improvement is quantitatively reflected in the reduction of the drug's IC_{50} value (half-maximal inhibitory concentration)—the concentration required to inhibit 50% cell viability. Upon conjugation with Trp-Cu NC, Dox's IC_{50} against MCF-7 cells decreased by approximately 3.6-fold, from 22.5 ± 3 μM to 6.2 ± 1 μM ($p < 0.006$) (Fig. 7(A) and Fig. S6A, ESI†). A lower IC_{50} indicates that the drug is effective at lower concentrations, potentially reducing systemic toxicity in patients.[61] These results demonstrate that the Trp-Cu NC-based nanocarrier not only enhances the potency of Dox but also shows superior performance compared to free Dox and other reported nano-drug carriers (Table 1).

Although free Dox exhibited comparable cytotoxicity toward both normal (IC_{50} = 19.2 ± 1.6 μM) and cancer cells (IC_{50} = 22.5 ± 3 μM), conjugation with Trp-Cu NC significantly reduced its toxicity toward normal cells, increasing the IC_{50} to 30.1 ± 2 μM ($p < 0.02$) (Fig. 7(B) and Fig. S6B, ESI†). This indicates that Trp-Cu

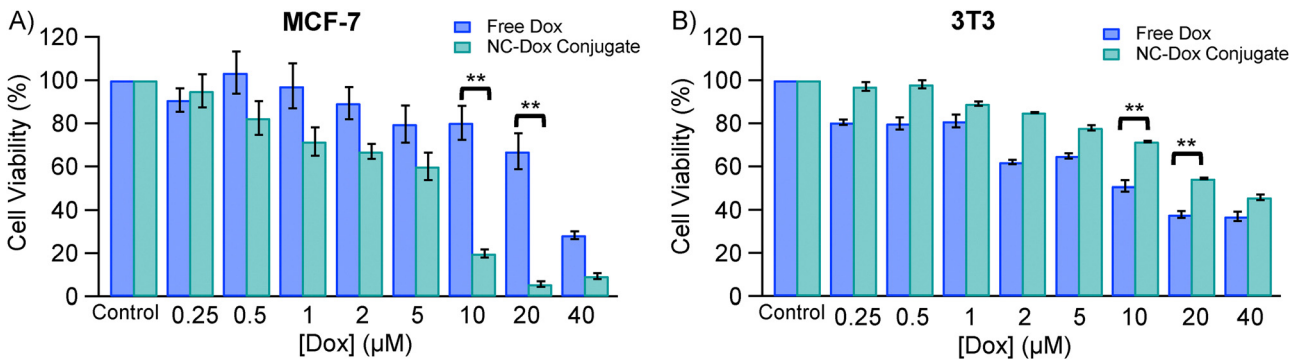

Fig. 7 Cell viability assay of free Dox (blue) and the Trp-Cu NC–Dox nanoconjugate (green) in (A) breast cancer (MCF-7) and (B) normal mouse fibroblast (3T3) cells. Statistical significance denoted by **($p < 0.002$).

Table 1 Comparison of IC_{50} improvement in the NC–Dox conjugate *vs.* free Dox

Nano-drug carriers	Cancer Cell	IC_{50} (Dox)	IC_{50} (NC–Dox)	[IC_{50} (Dox)/IC_{50} (NC–Dox)]	Ref.
Trp-Cu NC[a]	MCF-7	22.5 μM	6.2 μM	3.6	This work
Lysozyme-Au NC[b]	MCF-7	229 nM	155 nM	1.5	6
Transferrin-Cu NC[b]	MCF-7	1.23 μg mL^{-1}	0.6 μg mL^{-1}	2.0	25
Polysaccharide-Au NC[a]	MCF-7	43.7 μg mL^{-1}	60.5 μg mL^{-1}	0.7	62

[a] 24 h incubation. [b] 48 h incubation.

NC not only enhances the drug's therapeutic efficacy against cancer cells but also mitigates its harmful effects on healthy cells, thereby minimizing potential side effects. The underlying mechanism likely stems from the pH-sensitive nature of the drug release. Cancer cells typically exhibit a more acidic extracellular microenvironment compared to normal cells,[46,47] which promotes the release of Dox from the nanoconjugate under acidic conditions. In contrast, the neutral physiological pH (~7.4) of normal cells does not facilitate significant drug release, thereby reducing cytotoxicity toward healthy tissues. These findings underscore the potential of Trp-Cu NC as a smart nano-drug carrier capable of selectively releasing Dox to cancer cells while sparing normal cells. Such selective delivery could improve therapeutic outcomes and reduce the need for high doses of free Dox, commonly used in conventional chemotherapy, ultimately minimizing adverse side effects for cancer patients.

4. Conclusions

In summary, Trp-Cu NC demonstrated strong potential as an efficient nano-drug carrier for the targeted release of Dox to cancer cells. The drug-binding interaction and pH-responsive release were characterized using steady-state and time-resolved FRET analyses. At neutral pH, Trp-Cu NC formed a stable nanoconjugate with Dox, resulting in large rod-shaped particles in a 'FRET ON' state. This indicated high drug-binding efficiency and a strong interaction between the nanocluster and Dox. When exposed to an acidic environment (pH 5.5), mimicking the tumor microenvironment, the nanoconjugate underwent a significant reduction in particle size (~2.7 ± 0.1 nm), approximating that of the free Trp-Cu NC. This change, accompanied by an increase in the fluorescence lifetime of the nanocluster and a transition to the 'FRET OFF' state, confirmed the release of the drug. Cytotoxicity assays further validated that the Trp-Cu NC carrier enhances Dox's therapeutic efficacy by enabling selective cancer cell death at relatively low drug concentrations, while reducing toxicity to normal cells. This selective action decreases adverse effects on healthy tissues—an essential requirement for effective cancer therapy. Collectively, these findings underscore the potential of Trp-Cu NC as a promising nanoplatform for advancing cancer treatment strategies.

Author contributions

Aarya: data curation, formal analysis, methodology, writing – original draft. Anna Sebastian: data curation, formal analysis, writing – original draft. Kavya P.: data curation, formal analysis, writing – original draft. Indrajit Bhattacharjee: data curation, formal analysis. Abhishek S. Shekhawat: data curation. Bibhu Ranjan Sarangi: formal analysis, methodology. Supratik Sen Mojumdar: conceptualization, funding acquisition, methodology, supervision, writing – original draft, formal analysis.

Data availability

Data are available from the authors upon reasonable request.

Conflicts of interest

There are no conflicts to declare.

Acknowledgements

Aarya & K. P. thank UGC and A. S. thanks CSIR, Government of India, for providing fellowships. S. S. M. thanks SERB, Government of India (project no. CRG/2022/007366), and IIT Palakkad for financial assistance. S. S. M. thanks the central instrumentation facility (CIF) at IIT Palakkad for FTIR, TCSPC & FESEM measurements, SRM Institute of Science and Technology for HRTEM measurements and PSG Institute of Advanced Studies for DLS and Zeta potential measurements.

References

1 C. Frick, H. Rumgay, J. Vignat, O. Ginsburg, E. Nolte, F. Bray and I. Soerjomataram, *Lancet Global Health*, 2023, **11**, e1700–e1712.
2 S. Gavas, S. Quazi and T. M. Karpiński, *Nanoscale Res. Lett.*, 2021, **16**, 173.
3 M. Ashrafizadeh, K. Hushmandi, S. Mirzaei, S. Bokaie, A. Bigham, P. Makvandi, N. Rabiee, V. K. Thakur, A. P. Kumar, E. Sharifi, R. S. Varma, A. R. Aref, M. Wojnilowicz, A. Zarrabi, H. Karimi-Maleh, N. H. Voelcker, E. Mostafavi and G. Orive, *Bioeng. Transl. Med.*, 2023, **8**, e10325.
4 J. Prados, C. Melguizo, R. Ortiz, C. Velez, P. J. Alvarez, J. L. Arias, M. A. Ruiz, V. Gallardo and A. Aranega, *Anti-Cancer Agents Med. Chem.*, 2012, **12**, 1058–1070.
5 M. Sarparast, A. Noori, H. Ilkhani, S. Z. Bathaie, M. F. El-Kady, L. J. Wang, H. Pham, K. L. Marsh, R. B. Kaner and M. F. Mousavi, *Nano Res.*, 2016, **9**, 3229–3246.
6 S. Chattoraj, A. Amin, B. Jana, S. Mohapatra, S. Ghosh and K. Bhattacharyya, *ChemPhysChem*, 2016, **17**, 253–259.
7 S. C. Piscitelli, K. A. Rodvold, D. A. Rushing and D. A. Tewksbury, *Clin. Pharmacol. Ther.*, 1993, **53**, 555–561.
8 S. Kamba, M. Ismail, S. Hussein-Al-Ali, T. Ibrahim and Z. Zakaria, *Molecules*, 2013, **18**, 10580–10598.
9 D. Florou, C. Patsis, A. Ardavanis and A. Scorilas, *Cancer Biol. Ther.*, 2013, **14**, 587–596.
10 S. Aryal, J. J. Grailer, S. Pilla, D. A. Steeber and S. Gong, *J. Mater. Chem.*, 2009, **19**, 7879.
11 H. Nasrollahpour, B. J. Sánchez, M. Sillanpää and R. Moradi, *ACS Appl. Nano Mater.*, 2023, **6**, 12609–12672.
12 G. Yang, Z. Wang, F. Du, F. Jiang, X. Yuan and J. Y. Ying, *J. Am. Chem. Soc.*, 2023, **145**, 11879–11898.
13 S. Kundu, M. Ghosh and N. Sarkar, *Langmuir*, 2021, **37**, 9281–9301.
14 A. L. Villela Zumaya, R. Mincheva, J.-M. Raquez and F. Hassouna, *Polymers*, 2022, **14**, 1188.

15 A. Sebastian, Aarya, B. R. Sarangi and S. Sen Mojumdar, *J. Photochem. Photobiol., A*, 2023, **436**, 114378.
16 P. L. Xavier, K. Chaudhari, A. Baksi and T. Pradeep, *Nano Rev.*, 2012, **3**, 14767.
17 R. Tumskiy, B. Khlebtsov, A. Tumskaia, S. Evstigneeva, E. Antoshkina, A. Zakharevich and N. G. Khlebtsov, *Int. J. Mol. Sci.*, 2023, **24**, 8306.
18 C.-Y. Chang, Y.-R. Wu, T.-H. Tseng, J.-H. Su, Y.-S. Wang, F.-Y. Jen, B.-R. Chen, C.-L. Huang and J.-C. Chen, *Nanomaterials*, 2023, **13**, 2338.
19 Aarya, T. Thomas, B. R. Sarangi and S. Sen Mojumdar, *ACS Omega*, 2023, **8**, 14630–14640.
20 P. Kavya, Aarya, A. Sebastian and S. Sen Mojumdar, *Sens. Actuators, B*, 2024, **401**, 134923.
21 Y. Chen, M. L. Phipps, J. H. Werner, S. Chakraborty and J. S. Martinez, *Acc. Chem. Res.*, 2018, **51**, 2756–2763.
22 Y. Lai, X. Teng, Y. Zhang, H. Wang, P. Pang, C. Yang, C. J. Barrow and W. Yang, *Anal. Methods*, 2019, **11**, 3584–3589.
23 Rashi, D. Bain, A. Devi, S. Chakraborty and A. Patra, *ACS Sustainable Chem. Eng.*, 2023, **11**, 1995–2004.
24 B. Casteleiro, F. Da Cruz-Boisson, P. Alcouffe, S. N. Pinto, J. M. Gaspar Martinho, M.-T. Charreyre, J. P. S. Farinha and A. Favier, *ACS Appl. Nano Mater.*, 2023, **6**, 11689–11698.
25 U. Goswami, A. Dutta, A. Raza, R. Kandimalla, S. Kalita, S. S. Ghosh and A. Chattopadhyay, *ACS Appl. Mater. Interfaces*, 2018, **10**, 3282–3294.
26 A. Yahia-Ammar, D. Sierra, F. Mérola, N. Hildebrandt and X. Le Guével, *ACS Nano*, 2016, **10**, 2591–2599.
27 D. Chen, Z. Luo, N. Li, J. Y. Lee, J. Xie and J. Lu, *Adv. Funct. Mater.*, 2013, **23**, 4324–4331.
28 T. Chen, B. He, J. Tao, Y. He, H. Deng, X. Wang and Y. Zheng, *Adv. Drug Delivery Rev.*, 2019, **143**, 177–205.
29 Q. Li, Y. Pan, T. Chen, Y. Du, H. Ge, B. Zhang, J. Xie, H. Yu and M. Zhu, *Nanoscale*, 2018, **10**, 10166–10172.
30 R. Ghosh, U. Goswami, S. S. Ghosh, A. Paul and A. Chattopadhyay, *ACS Appl. Mater. Interfaces*, 2015, **7**, 209–222.
31 W. Liu, J. Wang, S. Yuan, X. Chen and Q. Wang, *Angew. Chem., Int. Ed.*, 2021, **60**, 11430–11435.
32 S. Chakraborty and S. Mukherjee, *J. Phys. Chem. Lett.*, 2021, **12**, 3266–3273.
33 A. J. de Jesus and T. W. Allen, *Biochim. Biophys. Acta, Biomembr.*, 2013, **1828**, 864–876.
34 S. Khemaissa, S. Sagan and A. Walrant, *Crystals*, 2021, **11**, 1032.
35 S. Shahsavari, S. Hadian-Ghazvini, F. Hooriabad Saboor, I. Menbari Oskouie, M. Hasany, A. Simchi and A. L. Rogach, *Mater. Chem. Front.*, 2019, **3**, 2326–2356.
36 K. Anusuyadevi, S. P. Wu and S. Velmathi, *J. Photochem. Photobiol., A*, 2021, **421**, 113526.
37 Z. Dong, Y. Bi, H. Cui, Y. Wang, C. Wang, Y. Li, H. Jin and C. Wang, *ACS Appl. Mater. Interfaces*, 2019, **11**, 23840–23847.
38 X. Han, D.-E. Liu, T. Wang, H. Lu, J. Ma, Q. Chen and H. Gao, *ACS Appl. Mater. Interfaces*, 2015, **7**, 23760–23766.
39 B. Schuler, E. A. Lipman, P. J. Steinbach, M. Kumke and W. A. Eaton, *Proc. Natl. Acad. Sci. U. S. A.*, 2005, **102**, 2754–2759.
40 T. Ha, T. Enderle, D. F. Ogletree, D. S. Chemla, P. R. Selvin and S. Weiss, *Proc. Natl. Acad. Sci. U. S. A.*, 1996, **93**, 6264–6268.
41 L. Stryer, *Annu. Rev. Biochem.*, 1978, **47**, 819–846.
42 J. R. Lakowicz, *Principles of fluorescence spectroscopy*, Springer, New York, 3rd edn, 2006.
43 B. Schuler, A. Soranno, H. Hofmann and D. Nettels, *Annu. Rev. Biophys.*, 2016, **45**, 207–231.
44 L. Yuan, W. Lin, K. Zheng and S. Zhu, *Acc. Chem. Res.*, 2013, **46**, 1462–1473.
45 G. Yang, Y. Liu, J. Teng and C.-X. Zhao, *Biosensors*, 2021, **11**, 505.
46 M. H. Lee, J. H. Han, J. H. Lee, N. Park, R. Kumar, C. Kang and J. S. Kim, *Angew. Chem., Int. Ed.*, 2013, **52**, 6206–6209.
47 H. Hou, Y. Zhao, C. Li, M. Wang, X. Xu and Y. Jin, *Sci. Rep.*, 2017, **7**, 1759.
48 B. Delavari, F. Mamashli, B. Bigdeli, A. Poursoleiman, L. Karami, Z. Zolmajd-Haghighi, A. Ghasemi, S. Samaei-Daryan, M. Hosseini, T. Haertlé, V. I. Muronetz, Ø. Halskau, A. A. Moosavi-Movahedi, B. Goliaei, A. H. Rezayan and A. A. Saboury, *Sci. Rep.*, 2018, **8**, 17345.
49 L. Ma, F. Yang and J. Zheng, *J. Mol. Struct.*, 2014, **1077**, 87–100.
50 X. Tan and J. R. Caram, *J. Chem. Phys.*, 2023, **158**, 204705.
51 B. Wallace and P. J. Atzberger, *PLoS One*, 2017, **12**, e0177122.
52 C. C. Miller and J. Walker, *Proc. R. Soc. London, Ser. A*, 1997, **106**, 724–749.
53 J. D. A. Lin, O. V. Mikhnenko, J. Chen, Z. Masri, A. Ruseckas, A. Mikhailovsky, R. P. Raab, J. Liu, P. W. M. Blom, M. A. Loi, C. J. García-Cervera, I. D. W. Samuel and T.-Q. Nguyen, *Mater. Horiz.*, 2014, **1**, 280–285.
54 R. Khandelia, S. Bhandari, U. N. Pan, S. S. Ghosh and A. Chattopadhyay, *Small*, 2015, **11**, 4075–4081.
55 H. Hashemi and H. Namazi, *Mater. Today Commun.*, 2021, **28**, 102593.
56 S. Das, S. Rakshit and A. Datta, *J. Phys. Chem. C*, 2021, **125**, 15396–15404.
57 D. Chudoba, M. Jażdżewska, K. Łudzik, S. Wołoszczuk, E. Juszyńska-Gałązka and M. Kościński, *Int. J. Mol. Sci.*, 2021, **22**, 12003.
58 M. Kanamala, W. R. Wilson, M. Yang, B. D. Palmer and Z. Wu, *Biomaterials*, 2016, **85**, 152–167.
59 D. Rout, S. Sharma, P. Agarwala, A. K. Upadhyaya, A. Sharma and D. K. Sasmal, *ACS Omega*, 2023, **8**, 3114–3128.
60 X. Yang, G. Zhang, Y. Li, Z. Liu, X. Gong, B. Gao, G. Zhang, Y. Cui and G. Sun, *RSC Adv.*, 2015, **5**, 22455–22462.
61 C. Berrouet, N. Dorilas, K. A. Rejniak and N. Tuncer, *Bull. Math. Biol.*, 2020, **82**, 68.
62 N. Li, Y. Chen, Y.-M. Zhang, Y. Yang, Y. Su, J.-T. Chen and Y. Liu, *Sci. Rep.*, 2014, **4**, 4164.